Available online at www.sciencedirect.com
ScienceDirect
Catalysis Today 133–135 (2008) 331–338
CATALYSIS TODAY
www.elsevier.com/locate/cattod

A study of *n*-hexane hydroisomerization catalyzed with the $Pt/H_3PW_{12}O_{40}$/Zr-MCM-41 catalysts

L.F. Chen [a,*], L.E. Noreña [b,*], J.A. Wang [a], X.L. Zhou [c], J. Navarrete [d], I. Hernández [b], A. Montoya [d], P. Pérez Romo [d], P. Salas [e], S. Castella Pergher [f]

[a] *ESIQIE, Instituto Politécnico Nacional, Col. Zacatenco, 07738 México, D.F., Mexico*
[b] *Departamento de Ciencias Básicas, Universidad Autónoma Metropolitana-A, Av. San Pablo 180, Col. Reynosa-Tamaulipas, 02200 México, D.F., Mexico*
[c] *Petroleum Processing Research Center, East China University of Science and Technology, Shanghai 200237, China*
[d] *Grupo de Molecular Ingeniería, Instituto Mexicano del Petróleo, Eje Lázaro Cárdenas 152, 07730 México, D.F., Mexico*
[e] *Centro de Física Aplicada y Tecnología Avanzada, Universidad Nacional Autónoma de México, A.P. 1-1010, 76000 Querétaro, Mexico*
[f] *Universidad Regional Intergrada do Alto Uruguai e das Missoes, Campus Erechim, URI, C.P. 743, Brazil*

Available online 7 February 2008

Abstract

A series of Zr-modified MCM-41 mesoporous materials with a variety of Si/Zr molar ratios were synthesized by the surfactant-templated method. Textural properties, crystalline structure and surface acidity were characterized by X-ray diffraction (XRD), low-temperature N_2 physisorption isotherms, solid-state nuclear magnetic resonance (MAS-NMR), UV–visible spectroscopy, and Fourier-transform infrared (FTIR) spectroscopy of pyridine adsorption techniques. Both the as-made and the calcined materials show the typical MCM-41 structure with hexagonal mesochannels. The structural regularity varies with zirconium content in the materials. A proper amount of zirconium ions incorporated into the Si framework may noticeably improve the structural order, but high zirconium content leads to the reduction of the structural regularity. The mean pore diameter of the materials increases from 2.8 to 3.0, 3.8 and 4.5 nm as the Si/Zr molar ratio decreases from 25 to 15, 8 and 4, respectively. Meanwhile, the surface area and pore volume diminish with the increase of zirconium content. As $H_3PW_{12}O_{40}$ (referred as HPW) is dispersed on the Zr-MCM-41 materials, the Brönsted acidity is greatly enhanced: from four to eight times. Three forms of heteropolyanions: (i) bulk-like HPW particles, (ii) highly dispersed HPW clusters with deformed Keggin structure and (iii) HPW species with partially fragmented Keggin structure, are adopted by the HPW deposited on the Zr-MCM-41 solids, due to the different interactions between the heteropolyacid species and the support. The 1 wt.%Pt/25 wt.%HPW/Zr-MCM-41 catalysts show high activity for the *n*-hexane hydroisomerization reaction, with 100% selectivity to isohexanes at temperatures below 260 °C. Increasing the zirconium content generally leads to a higher *n*-hexane conversion but it lowers the selectivity to hexane isomers that might be related to the different pore diameter distribution and surface density of the Brönsted acid sites.

Keywords: Zr-MCM-41; Heteropolyacid; *n*-Hexane; Hydroisomerization; Catalyst

1. Introduction

The Si-based MCM-41 materials have large potential applications in the fine chemical industry, adsorption and separation processes, heterogeneous catalysis and in the petroleum refinery industry [1–5]. However, Si-based MCM-41 lacks Brönsted acidity and it exhibits only mild Lewis acidity, which is much weaker than that of microporous zeolites [6]. In acidic catalyzed reactions, such as the isomerization of hydrocarbons, when Si-MCM-41 is used either as catalyst or as catalyst support, its acidity needs to be enhanced [7].

Through two approaches, the surface acidity of the Si-MCM-41 materials can be enhanced: the first is the framework modification by incorporation of foreign ions like Al^{3+} and Zr^{4+} into the Si framework [8–10], and the second is surface grafting by the introduction of strong acid groups like SO_4^{2-} or heteropolyacids [3,11–15].

In the present work, the enhancement of the surface acidity of Si-MCM-41 by simultaneous modifications of the surface

* Corresponding authors.
E-mail addresses: chenlf2001@yahoo.com (L.F. Chen), lnf@correo.azc.uam.mx (L.E. Noreña).

0920-5861/$ – see front matter © 2008 Elsevier B.V. All rights reserved.
doi:10.1016/j.cattod.2007.12.115

and the framework is reported. Our aim was to introduce zirconium ions into the Si framework during the synthesis procedure and to disperse a heteropolyacid, $H_3PW_{12}O_{40}$, onto the surface of the Zr-MCM-41 support. After impregnation with a given amount of H_2PtCl_6, a series of 1 wt.%Pt/25 wt.%HPW/Zr-MCM-41 (referred as Pt/HPW/Zr-MCM-41) catalysts can be obtained.

The textural properties including surface area, average pore diameter and pore size distribution of the Zr-MCM-41 solids were measured by the low-temperature N_2 physisorption method. The crystalline structures of the resultant mesoporous solids and Pt/HPW/Zr-MCM-41 catalysts were studied by using XRD, ^{31}P MAS-NMR and UV–visible spectroscopic techniques. The surface acidity of both, the Zr-MCM-41 support and the catalysts, were determined by using the *in situ* FTIR of pyridine adsorption method. The catalytic activity and selectivity of the catalysts were evaluated in the reaction of *n*-hexane isomerization in the presence of hydrogen at different conditions.

2. Experimental

2.1. Preparation of the Zr-MCM-41 supports

The Zr-MCM-41 solids were prepared using tetraethylorthosilicate (TEOS) as Si precursor and zirconium-*n*-propoxide (70% in propanol) as Zr source, along with cetyltrimethylammonium chloride (CTACl) as synthesis template. The typical preparation procedure of a Zr-MCM-41 sample with a molar ratio of Si/Zr = 25 is as follows: First of all, two solutions were prepared, the first solution was made by adding 1.77 ml of zirconium-*n*-propoxide and 22.8 ml of TEOS with stirring; the second solution was made by adding 11.3 g of CTACl into 110 ml of hot water (around 50 °C) with stirring, followed by the addition of 110 ml of $NH_3{\cdot}H_2O$ (28 wt.%). Then, the first solution was added, drop by drop, into the second solution. During the addition, the mixture was vigorously stirred for about 2 h, until a gel was formed. The resultant gel was loaded into a stoppered Teflon bottle without stirring and kept at 100 °C for 48 h. After cooling to room temperature, the resulting solid product was recovered by filtration and was washed for four times with 500 ml deionized water. The white solid obtained was dried in air at 80 °C for 24 h. Finally, the sample was calcined at 600 °C for 6 h in air. The heating rate was 1 °C/min. The samples were referred as Zr-MCM-41-*n*, where molar ratio *n* = Si/Zr = 25, 15, 8 and 4.

2.2. Preparation of the catalysts

The Zr-MCM-41 supports were first impregnated with 20 ml of a methanol solution containing a given amount of $H_3PW_{12}O_{40}$. The solvent was removed at 40 °C in a vacuum evaporator until dryness. Afterwards, the 25 wt.%HPW/Zr-MCM-41 solids were impregnated with 20 ml of a water solution containing H_2PtCl_6. The solvent was evaporated at 80 °C in a vacuum evaporator until a dried material with 1 wt.%Pt was obtained. The amounts of the $H_3PW_{12}O_{40}$ and the H_2PtCl_6 used depend upon the amount of the support. The dried catalysts were calcined at 300 °C in air for 2 h.

2.3. X-ray diffraction analysis

The low-angle X-ray diffraction patterns of the samples were measured in a D-500 SIEMENS diffractometer with a graphite secondary beam monochromator producing a monochromatic Cu Kα radisation, and the evaluation of the diffractograms was made by DIFFRAC/AT software. The scanning was made from 1.5° to 10°, with a 2θ step size of 0.02° and a step time of 2 s. In order to avoid the problem of illuminated area at low 2θ angles, all the samples were measured using the same sample holder. In this way, the hexagonal reflection (1 0 0) positions as well as the intensities are directly comparative. Position correction was made using the NIST standard reference material 675.

2.4. N_2 adsorption isotherms measurements

The specific surface area, pore volume and pore size distribution of the samples were measured in a Digisorb 2600 equipment by using low-temperature N_2 physisorption isotherms. Before the measurement, the sample was evacuated at 350 °C under vacuum condition. The surface area was calculated using the BET method based on the adsorption data within the partial pressure P/P_0 range from 0.01 to 1. The mesopore volume was determined from the N_2 adsorbed at a $P/P_0 = 0.4$.

2.5. Solid-state nuclear magnetic resonance (^{31}P MAS-NMR)

Solid-state ^{31}P MAS-NMR spectra were recorded on a Bruker 400 MHz spectrometer at a frequency of 79.49 MHz, 7.5 kHz spinning, using pulses at 90 s intervals and 4 mm zirconia rotors. The number of accumulations was 500. All the measurements were carried out at room temperature. For the ^{31}P analysis, H_3PO_4 was used as standard reference to obtain the chemical shift of the solid materials.

2.6. The diffuse reflectance UV–visible spectroscopic analysis (UV–vis)

The UV–vis diffuse reflectance spectra of the samples were collected on a Varian Cary 1G UV–visible spectrometer with an attached diffuse reflectance apparatus at room temperature after pre-treatment at 300 °C for 2 h. Scan control conditions: average time, 0.10 s; data interval, 1.00 nm; scan rate, 600 nm/min; absorption mode; wavelength range, 190–900 nm.

2.7. FTIR spectroscopy of pyridine adsorption

To evaluate and analyze the strength and types of acid sites, pyridine adsorption on the samples was performed on a 170-SX Fourier-transform infrared (FTIR) spectrometer at different temperatures, ranging from 25 to 400 °C. Before pyridine

adsorption, each sample was heated to 300 °C for 60 min under vacuum, in order to eliminate the adsorbed water or impurities on the surface, and then cooled to room temperature. Afterwards, the solid wafer was exposed to pyridine, by breaking inside the spectrometer cell, a capillary containing 50 μl of liquid pyridine. The IR spectra were recorded at various conditions by increasing the cell temperature from 25 to 400 °C. The quantitative calculation of Lewis and Brönsted acid sites was made with respect to the area of the adsorption band at 1450 and 1540 cm^{-1}, respectively. The acid strength was determined with respect to the variation of the number of acid sites as a function of the temperature.

2.8. Catalytic evaluation

The catalytic reactions were carried out in a down-flow fixed-bed tubular reactor (i.d. 1.0 cm, 30 cm in length) in the presence of hydrogen at a 1 MPa total pressure. The catalyst loading was 0.2 g, the hydrogen/*n*-hexane molar ratio was 4 and the reaction temperature varied from 220 to 320 °C. The weight hourly space velocity (WHSV) was 2.4. Before the reaction, the catalysts were reduced at 300 °C for 2 h using hydrogen in order to reduce the platinum oxide to metallic Pt. The products distribution was analyzed using an on-line analytical system (GC Varian 3300) equipped with a flame ionization detector (FID).

3. Results and discussion

3.1. Structure and textural properties of the Zr-MCM-41 supports

Fig. 1 shows the XRD patterns of the calcined solids with different Si/Zr molar ratios. Four peaks corresponding to the (1 0 0), (1 1 0) (2 0 0) and (2 1 0) reflections of the materials are observed, which are indexed to the hexagonal structure of typical mesoporous MCM-41 materials. The intensities of the diffraction peaks are noticeably increased compared to that of the as-made samples (not shown), due to the removal of the occluded surfactant molecules during the calcination process and to the improvement of the structural order after calcination. It is noteworthy that the intensities of the diffraction peaks vary with the zirconium content. The calcined sample with a Si/Zr molar ratio 15 shows the highest intensity of the (1 0 0) reflection, while, the sample with Si/Zr = 4 shows the lowest intensity, indicating that the zirconium content in the solid has an important effect on the structural ordering of the resultant materials. Therefore, after the incorporation of a proper amount of zirconium ions into the framework, the structural ordering can be improved. With a too low zirconium content, this improvement is not significant (i.e., Si/Zr = 25); however, a too high zirconium content may result in a poor structural regularity, as the case of Si/Zr = 4, due to partial collapsing of the pore structure as a consequence of large structural strain. In this series of Zr-MCM-41 samples, the molar ratio Si/Zr = 15 is the optimal, corresponding to the best structural ordering.

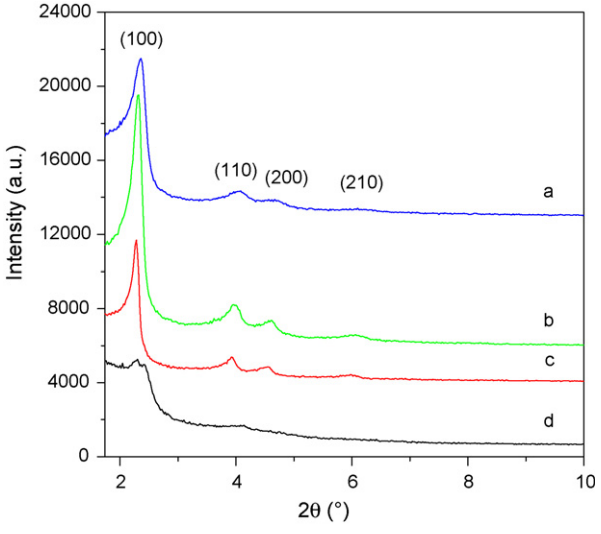

Fig. 1. XRD patterns of the calcined Zr-MCM-41 samples: (a) Si/Zr = 25, (b) Si/Zr = 15, (c) Si/Zr = 8 and (d) Si/Zr = 4.

Table 1 shows the related structural data derived from the XRD analysis and textural property measurements. As the Si/Zr molar ratio decreases from 25 to 15 and 8, the (1 0 0) peak position slightly shifts towards smaller values, thus the distance of the (1 0 0) interplanar spacing and the lattice cell parameter (a_0) increase. The wall thickness (t) slightly increases with the increasing of the zirconium content, indicating the incorporation of zirconium into the framework (Table 1).

The N_2 adsorption–desorption properties of the samples of Zr-MCM-41 materials calcined at 600 °C were determined by the N_2 physical adsorption–desorption isotherms method. Based on the IUPAC classification, the hysteresis loops belong to type IV profiles. A sharp step at a relative pressure P/P_0 around 0.2–0.3 was observed in all the samples, which reveals the highly ordered mesoporous systems. The pore diameter (d_p) corresponding to the main peak in the pore size distribution profile slightly increases with the zirconium content until the Si/Zr molar ratio reaches 4. However, The average pore diameter (d_{pa}) calculated from the wide range between 1.5 and 100 nm, linearly increases from 2.79 to 3.00, 3.75 and 4.44 nm as the Si/Zr molar ratio decreases from 25 to 15, 8 and 4, respectively, indicating that some mesopores might collapse in the solids with high zirconium content. At low zirconium contents, there is a narrow pore size distribution while at high zirconium contents the pore size distribution becomes broader. The high zirconium content also leads to the reduction of both, the surface area and the pore volume (Table 2).

Table 1
Structural data derived from XRD and BET measurements of the Zr-MCM-41 materials

Si/Zr	*h k l*	2θ (°)	$d_{1\,0\,0}$ (nm)	a_0 (nm)	d_p (nm)	t (nm)
25	1 0 0	2.36	3.74	4.32	2.40	1.92
15	1 0 0	2.32	3.81	4.40	2.46	1.94
8	1 0 0	2.28	3.88	4.48	2.49	1.99
4	1 0 0	2.30	3.84	4.44	2.51	1.93

Table 2
Surface area, average pore diameter and pore volume of the Zr-MCM-41 materials

Si/Zr	Surface area (m^2/g)	Average pore diameter (nm)	Pore volume (cm^3/g)
25	1019.1	2.79	0.99
15	892.2	3.00	0.92
8	677.9	3.75	0.89
4	448.5	4.44	0.75

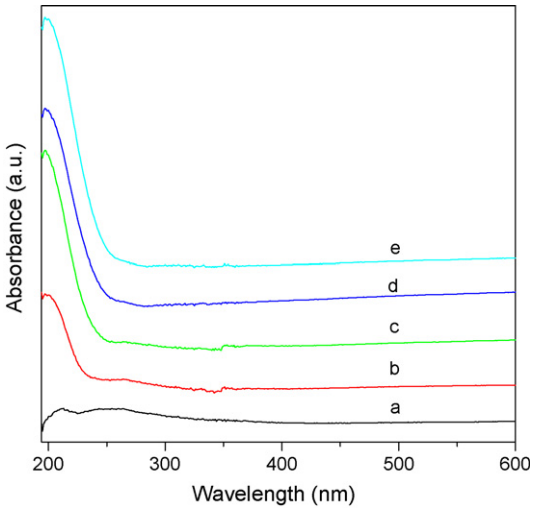

Fig. 2. The UV–visible spectra of the Zr-MCM-41 samples calcined at 600 °C: (a) Si-MCM-41, (b) Si/Zr = 25, (c) Si/Zr = 15, (d) Si/Zr = 8 and (e) Si/Zr = 4.

Fig. 2 illustrates the UV–visible spectra of the calcined Zr-MCM-41 solids along with that of the Si-MCM-41 sample as reference. The band around 200 nm is attributable to the charge-transfer transition from an oxygen ion to a Zr(IV) ion [16,17], corresponding to the excitation of electrons from the valence band (2p character in O) to the conduction band (4d character in Zr). The Si-MCM-41 sample (Fig. 3a) does not present any peak in the given range. Usually Zr ions in the perovskite-type $SiZrO_3$ show an absorption band around 240 nm in monoclinic ZrO_2 and an absorption band at around 300 nm in octahedral Zr^{4+} [18]. Our results suggest that the zirconium ions in the Zr-MCM-41 samples are in a different state from that in a pure ZrO_2 solid. This is another strong evidence of zirconium incorporation into the framework of the mesoporous materials. The band intensity increases as the Si/Zr ratio decreases, once again, indicating that more zirconium ions are incorporated into the Si framework at higher zirconium contents.

3.2. Structure and surface acidity of the Pt/HPW/Zr-MCM-41 catalysts

The XRD patterns of the Pt/HPW/Zr-MCM-41 catalysts are shown in Fig. 3. The intensity of the main reflection corresponding to the $d_{1\,0\,0}$ spacing is decreased in comparison to that of the bare support (Fig. 3a), indicating that the long-range order of the Zr-MCM-41 solids is reduced after the heteropolyacid loading. It is also seen that in the high 2θ range the XRD patterns exhibit rather wide peaks, strongly indicating the formation of highly dispersed heteropolyacid species on the support, therefore, the HPW cluster size is very fine (Fig. 3b).

The UV–visible spectra of the Pt/HPW/Zr-MCM-41 catalysts are shown in Fig. 4. Two peaks can be observed at around 202 and 254 nm, respectively. The absorption band at 254 nm is assigned to the $O^{2-} \rightarrow W^{6+}$ charge transfer of the polyoxotungstate at the W=O bond [8,12]. Bulk HPW shows absorption bands at approximately 220 and 350 nm (not shown). The shift of the band positions towards the high-energy direction in the HPW supported solids, for example, from 350 to 254 nm and from 220 to 202 nm, indicates the high dispersion of the heteropolyacids on the Zr-MCM-41 support or the possible deformation of the Keggin structure.

The Keggin structure of the Pt/HPW/Zr-MCM-41 samples with various Si/Zr molar ratios was also studied by the ^{31}P MAS-NMR spectroscopic technique. Several peaks at

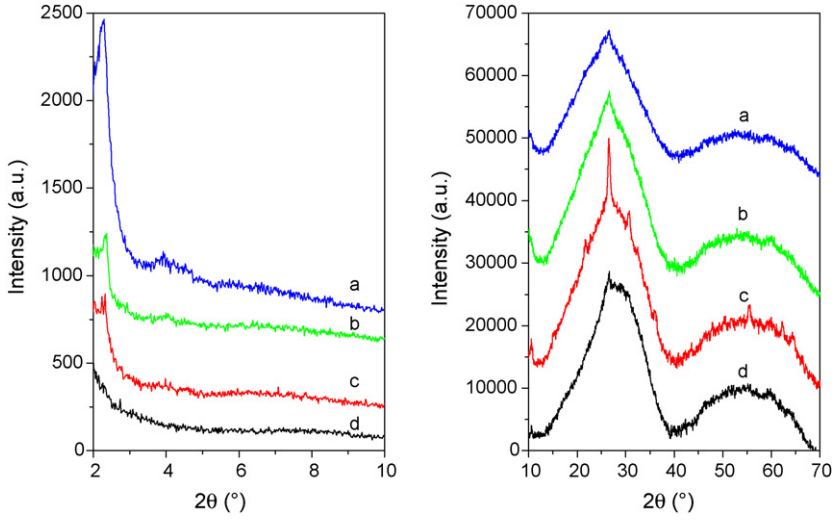

Fig. 3. XRD patterns of the Pt/HPW/Zr-MCM-41 catalysts: (a) Si/Zr = 25, (b) Si/Zr = 15, (c) Si/Zr = 8 and (d) Si/Zr = 4.

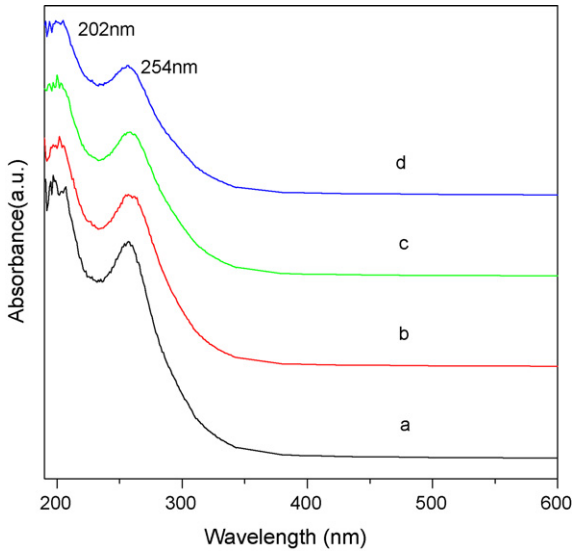

Fig. 4. The UV–visible spectra of the Pt/HPW/Zr-MCM-41 catalysts: (a) Si/Zr = 25, (b) Si/Zr = 15, (c) Si/Zr = 8 and (d) Si/Zr = 4.

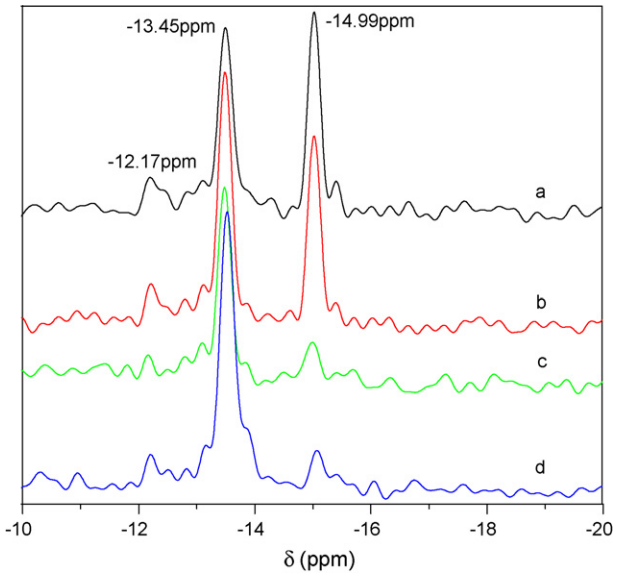

Fig. 5. The spectra of ^{31}P MAS-NMR of the catalysts: (a) 1 wt.%Pt/25 wt.%HPW/Zr-MCM-41 (Si/Zr = 25), (b) 1 wt.%Pt/25 wt.%HPW/Zr-MCM-41 (Si/Zr = 15), (c) 1 wt.%Pt/25 wt.%HPW/Zr-MCM-41 (Si/Zr = 8) and (d) 1 wt.%Pt/25 wt.%HPW/Zr-MCM-41 (Si/Zr = 4).

approximately −12.2, −13.5 and −14.9 ppm were observed, as shown in Fig. 5. Pure $H_3PW_{12}O_{40}$ exhibits only a single sharp peak, around −15 ppm (not shown). It has been reported that for $H_3PW_{12}O_{40}$ supported on TiO_2, four peaks at −4, −8, −11 and −13 ppm are formed, which have been assigned to adsorbed phosphorus species deriving from a highly fragmented Keggin unit, a partially fragmented and a deformed Keggin structure interacting with surface hydroxyl groups, respectively [19]. Based on the mentioned information, we infer that in our catalysts, heteropolyanions with different structures were formed: the peak at −14.96 ppm resulted from an unchanged bulk-like $H_3PW_{12}O_{40}$ structure, which indicates that some bulk-like $H_3PW_{12}O_{40}$ clusters or highly dispersed small particles exist on the surface of the Zr-MCM-41 support; the peak around −13.5 ppm indicates that the Keggin structure was deformed due to interacting with surface hydroxyl groups of the support; while the small peak at −12.17 ppm can be attributed to defect Keggin species due to the partial fragmentation of the Keggin structure, caused by the strong interaction with the support.

The formation of the heteropolyanions with different forms on the support was affected by the zirconium content. As the Si/Zr molar ratio decreased from 25 to 15, 8 and 4, the intensity of the resonance band at −14.96 ppm also significantly decreased, instead, the intensity of the resonance band around 13.5 ppm was generally increased. These variations reflect the changes of the amount of the different forms of the heteropolyanions on the support. Increasing the zirconium content brings about more highly dispersed heteropolyanion species interacting with the support and less bulk-like $H_3PW_{12}O_{40}$ clusters.

The acidity was determined by *in situ* FTIR of pyridine adsorption. Fig. 6 shows the *in situ* FTIR spectra of the pyridine adsorption on the Pt/HPW/Zr-MCM-41 catalyst with a Si/Zr molar ratio 4. Lewis acid sites (noted as L) exist on the surface of all the samples as characterized by the bands at 1445, 1579 and 1595 cm^{-1} in all the spectra [20–22]. It is noted that a hydrogen-bounded bond usually appears around 1435–1445 cm^{-1}, in most cases it is seen as a shoulder of the Lewis peak due to their close position [23,24]. In the present work, the hydrogen-bounded bond and the L acid bond might overlap due to a slight unsymmetry of the peak shape and such a shoulder was not clearly observed. The band corresponding to the vibration of pyridine associated with both, Lewis and Brönsted acid sites, is observed at 1490 cm^{-1} (noted as B + L acid sites). The absorption bands at 1545 and 1637 cm^{-1} confirm the presence of Brönsted acid sites (noted as B) in the samples [20–24]. When the catalysts are heated from 25 to 100 °C inside the IR cell under vacuum, the intensities of all the bands corresponding to Lewis acid sites are strongly reduced, whereas the Brönsted acid sites remain almost unchanged.

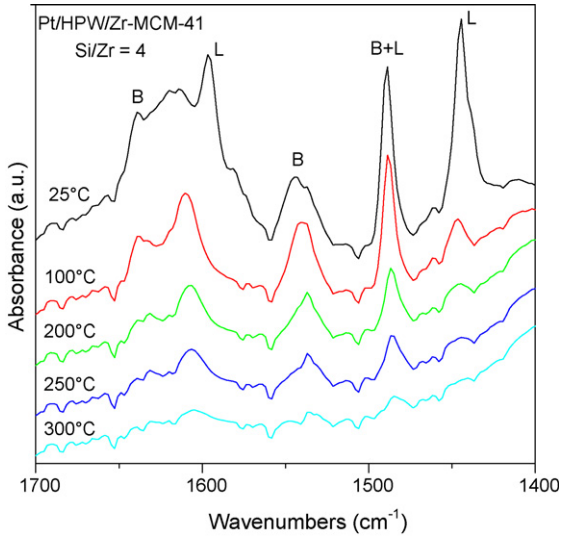

Fig. 6. *In situ* FTIR spectra of the pyridine adsorption on the catalyst with Si/Zr = 4 at various temperatures.

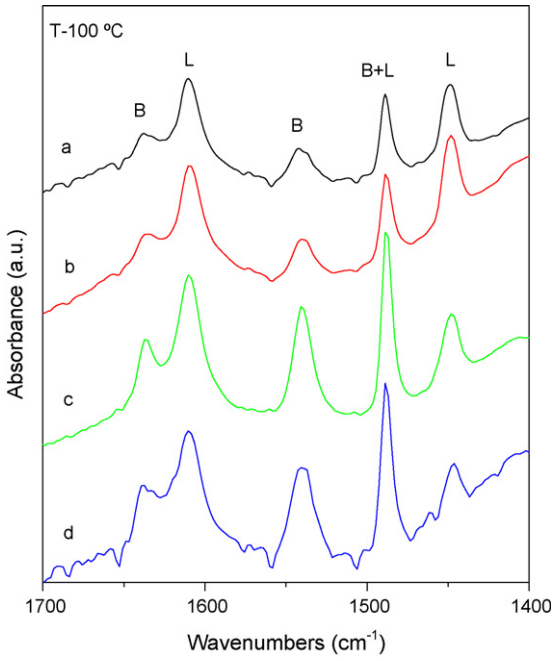

Fig. 7. *In situ* FTIR spectra of the pyridine adsorption on the various catalysts. The spectra were recorded at 100 °C under vacuum condition: (a) Si/Zr = 25, (b) Si/Zr = 15, (c) Si/Zr = 8 and (d) Si/Zr = 4.

After calcination at 300 °C, the bands are still visible in the sample with high zirconium content.

The zirconium content has an important effect on the surface acidity of the catalysts. Fig. 7 shows the FITR spectra of the pyridine adsorption on the different catalysts recorded at 100 °C. It is very clear that both, the Lewis and the Brönsted acidity linearly increase as the zirconium content increases.

In the pure Zr-MCM-41 support, both, Lewis and Brönsted acid sites are also formed. However, after heteropolyacid impregnation, the number of Brönsted acid sites is greatly enhanced. For example, for the catalyst with a support of Si/Zr = 25, the Brönsted acid sites are 106 μmol/g, which is four times higher than that of the non-impregnated support, where only 26 μmol/g Brönsted acid sites were achieved. It is also noteworthy that the acid strength is also significantly improved after $H_3PW_{12}O_{40}$ impregnation. The acid strength is relatively high for high zirconium content samples, i.e., Si/Zr = 4. Combining the information obtained from Fig. 5 and from Fig. 7, it is possible to conclude that high zirconium content results in a strong interaction between the dispersed heteropolyanion species and the support, leading to a strong deformation of the Keggin structure, thus enhancing the acidity.

3.3. Catalytic activity and selectivity

The catalytic evaluation shows that the Pt/HPW/Zr-MCM-41 catalysts are very active for *n*-hexane isomerization in the presence of hydrogen. The *n*-hexane conversion increases by increasing the reaction temperature (Fig. 8). The selectivity to isohexanes reaches 100% at a reaction temperature below 260 °C. At higher temperatures, side reactions such as cracking occur, lowering the selectivity to isomers (Fig. 9).

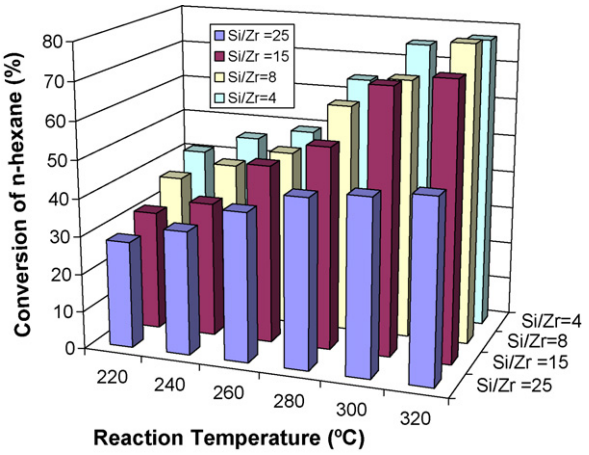

Fig. 8. *n*-Hexane conversion as function of the reaction temperature over the different catalysts.

Zirconium content has a significant influence on the catalytic activity and the selectivity. Largely, the catalytic activity increases as the Si/Zr molar ratio decreases, the catalyst with Si/Zr = 4 shows the highest catalytic activity at all the conversion levels, which can be explained by the surface acidity. As shown in Figs. 6 and 7, the catalyst with the higher zirconium content has a larger number of Brönsted acid sites and also stronger acidity, therefore an overall higher catalytic activity. However, it is noteworthy that the selectivity to isohexanes is low for the catalyst with high zirconium content, i.e., Si/Zr = 4. Strong acidity may favour the cracking reaction at high temperatures, which lowers the isomerization selectivity. Taking into account both, catalytic activity and selectivity, the molar ratio of Si/Zr should be bigger than 4, optimally between 15 and 8 in our experimental conditions. Too high or too low zirconium content in the support may lead to unbalance between metallic and acidic functions, which is unbeneficial to the enhancement of catalytic activity or selectivity.

In the products, isohexanes like 2-methylpentane (2MP), 3-methylpentane (3MP), 2,3-dimethylbutane (23DMB) and 2,2-dimethylbutane (22DMB) are formed (Tables 3 and 4).

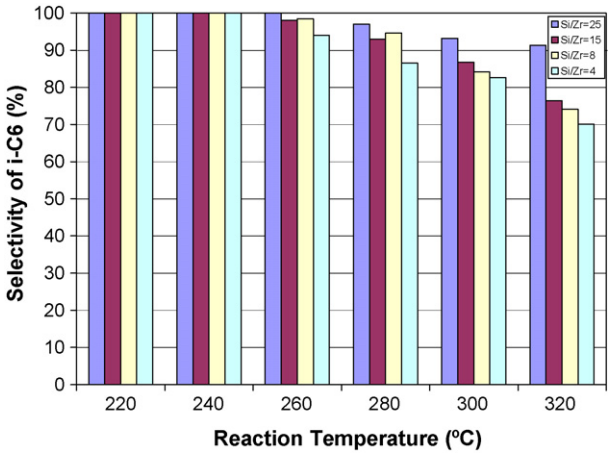

Fig. 9. Isohexanes selectivity as function of the reaction temperature over the different catalysts.

Table 3
Conversion, isohexanes selectivity and products selectivity at 240 °C[a]

Si/Zr	Conv. (%)	*S* (%)	Products selectivity (%)			
			2MP	3MP	23DMB	22DMB
25	32.8	100	57.0	35.1	7.9	0
15	35.7	100	57.7	26.7	5.6	0
8	42.1	100	53.2	31.8	12.4	0
4	46.0	100	55.4	34.4	10.2	0

[a] Conv.: *n*-hexane conversion; *S*: isohexanes selectivity.

The selectivity to 2MP and 3MP is predominant compared to that to 23DMB and 22DMB for all the conversion levels. The yields of dibranched products are less than 17% at the optimal temperature. The selectivity to 2MP and 3MP slightly decreases with increasing the reaction temperature, while, the selectivity to 23DMB and 22DMB slightly increases, indicating that 2MP and 3MP are likely to be precursors of the dibranched isomers.

Formation of 22DMB depends on the *n*-hexane conversion: higher hexane conversion or higher reaction temperature favours 22DMB formation. It has been reported that skeletal rearrangement of *n*-hexane can proceed through a protonated cyclopropane carbenium ion intermediate pathway [25]. Ring-opening of these intermediates easily produces the monomethylpentane isomers 2MP and 3MP. This is the reason why 2MP and 3MP are predominant for all the conversion levels. However, in the formation of the dibranched C_6 isomers, two successive steps of protonated cyclopropane intermediates are required. Obviously, high concentration of such intermediates produced at high conversion is favourable for the formation of dibranched isomers. Due to the difficulty in transforming a more stable tertiary carbocation ($(CH_3)_2$–CH^+–CH_2–CH_2–CH_3) into a less stable secondary carbocation ($(CH_3)_3C$–CH^+–CH_3), or the transformation from 23DMB into 22DMB by methyl shift, 22DMB remains below the thermodynamic value even at high conversion.

When comparing the distribution of each isomer product achieved by the various catalysts, it is found that high zirconium content seems to be in favour of the formation of dibranched isomers. This might be related to a different pore diameter distribution and to the surface density of the Brönsted acid sites. As reported in Table 2, the samples with Si/Zr = 8 and 4 show a larger pore diameter which is beneficial to structural rearrangement, required for the formation of large-size dibranched products and to fast diffusion through the mesochannels. On the other hand, the catalysts with high zirconium content present high surface density of Brönsted acid sites due to both, a lower surface area and a bigger number of Brönsted acid sites on these samples. Although strong Brönsted acidity may lead to cracking and lowering the selectivity, it definitely benefits the formation of the protonated cyclopropane carbenium ion intermediate and thus the formation of dibranched isomer products.

Table 4
Conversion, isohexanes selectivity and products selectivity at 280 °C[a]

Si/Zr	Conv. (%)	*S* (%)	Products selectivity (%)				
			2MP	3MP	23DMB	22DMB	C_p
25	44.7	97.0	50.7	30.8	7.8	4.0	3.0
15	53.6	93.0	44.3	31.4	8.5	5.1	7.0
8	60.7	94.6	46.0	28.1	9.9	6.8	5.4
4	64.7	86.5	40.0	25.4	9.3	4.5	13.5

[a] Conv.: *n*-hexane conversion; *S*: isohexanes selectivity; C_p: cracking products.

4. Conclusions

A proper amount of zirconium ions incorporated into the Si-MCM-41 framework may significantly enhance not only the structural ordering but also the Brönsted acidity, however, high Si/Zr molar ratios in the solid, i.e., Si/Zr = 4, may result in poor structural order. After impregnation with 25 wt.%$H_3PW_{12}O_{40}$, the Brönsted acidity is greatly enhanced to four to eight times relative to that of the bare Zr-MCM-41 support. The ^{31}P MAS-NMR spectroscopic analyses reveal that most of the Keggin structure in the dispersed heteropolyacid remains unchanged in the Zr-MCM-41 support with low zirconium content, which may transfer to species with distorted or partially fragmented Keggin structure due to the strong interaction between the Keggin units and the hydroxyl groups retained in the support with high zirconium content. The 1 wt.%Pt/25 wt.%HPW/Zr-MCM-41 catalysts are very active for the *n*-hexane hydroisomerization. The catalytic activity increases with increasing the zirconium content, however, high zirconium content lowers the selectivity to isohexanes. Increasing the reaction temperature promotes both, cracking reactions and formation of dibranched 22DMB isohexanes.

Acknowledgements

L.F. Chen wishes to thank the CONACyT scholarship for her doctoral study. Financial support obtained from CGPI-IPN-20050666, CONACyT (Mexico)-NSF (China) J110.426/2005 and the key international cooperative research project sponsored by the National Ministry of Science and Technology of China (no. 2004CB720603) is appreciated.

References

[1] A. Corma, Chem. Rev. 97 (1997) 2373.
[2] D.P. Serrano, J. Aguado, J.M. Escola, Ind. Eng. Chem. Res. 39 (2000) 1177.
[3] A. Ghanbari-Siahkali, A. Philippou, J. Dwyer, M.W. Anderson, Appl. Catal. A: Gen. 192 (2000) 57.
[4] J.H. Clark, Green Chem. 1 (1999) 1.
[5] K.M. Reddy, C. Song, Catal. Today 31 (1996) 137.
[6] A. Galarneau, D. Desplantie-Giscard, F. Di Renzo, F. Fajula, Catal. Today 68 (2001) 191.
[7] D. Trong On, D. Desplantrier-Giscard, C. Danumah, S. Kaliaguine, Appl. Catal. A: Gen. 222 (2001) 299.
[8] K. Nowińska, R. Fórmaniak, W. Kaleta, A. Wącław, Appl. Catal. A: Gen. 256 (2003) 115.
[9] R. Mokaya, J. Phys. Chem. B 104 (2000) 8279.
[10] L.F. Chen, L.E. Noreña, J. Navarrete, J.A. Wang, Mater. Chem. Phys. 97 (2006) 236.

[11] P. Salas, L.F. Chen, J.A. Wang, A. Armentáriz, M.L. Guzmán, J.A. Montoya, D.R. Acosta, Appl. Surf. Sci. 252 (2005) 1123.
[12] F. Marme, G. Coudurier, J.C. Védrine, Micropor. Mesopor. Mater. 22 (1998) 151.
[13] P.A. Jalil, M.A. Al-Daous, A.R.A. Al-Arfaj, A.M. Al-Amer, J. Beltramini, S.A.I. Barri, Appl. Catal. A: Gen. 207 (2001) 159.
[14] W. Yang, J. Billy, Y. Ben Taârit, J.C. Védrine, N. Essayem, Catal. Today 73 (2002) 153.
[15] T. Okuhara, N. Mizuno, M. Misono, Appl. Catal. A: Gen. 222 (2001) 63.
[16] S.I. Zabinsky, J.J. Rehr, A.A. Nkudinov, R.C. Albers, M.J. Eller, Phys. Rev. B 52 (1995) 2995.
[17] E. Rodríguez-Castellón, A. Jiménez-López, P. Marireles-Torres, D.J. Jones, J. Rozière, M. Trombetta, G. Busca, M. Lenarda, L. Storaro, J. Solid State Chem. 175 (2003) 159.
[18] E. Fernández López, V. Sánchez Escribano, M. Panizza, M.M. Carnasciali, G. Busca, J. Mater. Chem. 11 (2001) 1891.
[19] J.C. Edwards, C. Ivonne Thiel, B. Benac, J.F. Knifton, Catal. Lett. 51 (1998) 77.
[20] T. López, J. Navarrete, R. Gómez, O. Novaro, F. Figueras, H. Armendáriz, Appl. Catal. A: Gen. 125 (1995) 217.
[21] J.A. Wang, X. Bokhimi, López-Salinas, J. Mol. Catal. A: Chem. 137 (1999) 239.
[22] J. Sánchez-Valente, X. Bokhimi, F. Hernández, Langmuir 19 (2003) 3583.
[23] D. Srinivas, R. Srivastava, P. Ratnasamy, Catal. Today 96 (2004) 127.
[24] A. Sakthivel, S.E. Dapurkar, N.M. Gupta, S.K. Kulshreshtha, P. Selvam, Micropor. Mesopor. Mater. 65 (2003) 177.
[25] N. Essayem, Y. Ben Taârit, P.Y. Gayraud, G. Sapaly, C. Naccache, J. Catal. 204 (2001) 157.